

EVIDENCE FOR A WEAK WIND FROM THE YOUNG SUN*

BRIAN E. WOOD¹, HANS-REINHARD MÜLLER², SETH REDFIELD³, AND ERIC EDELMAN³

¹ Naval Research Laboratory, Space Science Division, Washington, DC 20375, USA; brian.wood@nrl.navy.mil

² Department of Physics and Astronomy, Dartmouth College, Hanover, NH 03755, USA

³ Astronomy Department, Van Vleck Observatory, Wesleyan University, 96 Foss Hill Drive, Middletown, CT 06459, USA

Received 2013 November 22; accepted 2013 December 17; published 2014 January 13

ABSTRACT

The early history of the solar wind has remained largely a mystery due to the difficulty of detecting winds around young stars that can serve as analogs for the young Sun. Here we report on the detection of a wind from the 500 Myr old solar analog π^1 UMa (G1.5 V), using spectroscopic observations from the *Hubble Space Telescope*. We detect H I Ly α absorption from the interaction region between the stellar wind and interstellar medium, i.e., the stellar astrosphere. With the assistance of hydrodynamic models of the π^1 UMa astrosphere, we infer a wind only half as strong as the solar wind for this star. This suggests that the Sun and solar-like stars do not have particularly strong coronal winds in their youth.

Key words: circumstellar matter – stars: winds, outflows – ultraviolet: stars

Online-only material: color figures

1. INTRODUCTION

Winds play an important role in stellar evolution for cool main sequence stars like the Sun, particularly with regard to stellar angular momentum. Interaction between stellar winds and the magnetic fields of rotating stars provides the mechanism by which angular momentum is transferred to the magnetized winds, slowing stellar rotation with time (Irwin et al. 2007; Denissenkov 2010; Spada et al. 2011; Gallet & Bouvier 2013). Understanding how this mechanism operates for stars of various ages requires knowledge of how winds evolve with time. Stellar wind evolution is also important for planetary studies, as stellar winds can play a role in eroding planetary atmospheres (Terada et al. 2009; Lammer et al. 2010; Khodachenko et al. 2012).

The solar wind, with a mass-loss rate of about $\dot{M}_\odot = 2 \times 10^{-14} M_\odot \text{ yr}^{-1}$ can be most simply understood as being due to thermal expansion from the hot ($T \sim 10^6$ K) corona (Parker 1958), though other acceleration mechanisms may be involved as well (Cranmer 2012). Young solar-like stars are known to be very active, with high coronal X-ray luminosities (Ribas et al. 2005), but this does not necessarily mean stronger coronal winds. The solar X-ray luminosity varies significantly during the course of the 11 yr solar activity cycle, but the total solar wind mass and momentum flux do not vary accordingly (Cohen 2011). Complicating things further, it is possible that mass loss from very active, frequently flaring stars may be dominated not by a constant quiescent wind but by sporadic coronal mass ejections (CMEs) associated with the frequent flares. To illustrate this, Drake et al. (2013) recently estimated a mass-loss rate of $\dot{M} = 150 \dot{M}_\odot$ for the young solar analog star π^1 UMa (G1.5 V) due to CMEs alone, assuming that the solar CME mass/flare relation can be applied to young stars with far more frequent and energetic flares.

The best way to address the issue of solar/stellar wind evolution is simply to detect and measure winds of various solar-

like stars and see how they vary with stellar age and activity. The problem is that coronal winds are very hard to detect remotely. The only established method of detection involves the analysis of stellar UV spectra from the *Hubble Space Telescope* (HST), specifically of the H I Ly α emission lines, in which absorption is sometimes observed from stellar astrospheres (the interaction regions between the stellar winds and the interstellar medium (ISM; Linsky & Wood 1996; Gayley et al. 1997; Wood et al. 2005b). The amount of absorption can be used to infer the stellar wind strength (Wood et al. 2002, 2005a).

To date, there are only eight detections of astrospheric absorption for main sequence stars with the spectral types of G or K, which can be considered solar-like (Wood et al. 2005a). These data suggest that wind strength does increase with coronal X-ray emission, which would indicate that young, active stars do have stronger coronal winds. However, the most active star in the sample, the binary ξ Boo (G8 V+K4 V), seems inconsistent with this relation, with a surprisingly low mass-loss rate of only $5 \dot{M}_\odot$, and with some evidence that it is actually the less active K4 V secondary that is largely responsible for the wind (Wood & Linsky 2010). This suggests that perhaps the wind/X-ray correlation fails for the youngest, most active stars. However, such a surprising conclusion requires verification, preferably for a star without the binarity issues of ξ Boo.

Better young solar analogs have been observed in the past, such as χ^1 Ori (Wood et al. 2005b), but they have not provided astrospheric detections. Unfortunately, a nondetection does not generally provide a meaningful upper limit to stellar wind strength in most cases, because one likely explanation for many nondetections is that the star is surrounded by a fully ionized ISM, which is quite prevalent within the Local Bubble (Lallement et al. 2003). Thus, we truly do require an astrospheric detection for progress to be made and here we report just such a detection for the aforementioned young star π^1 UMa.

2. DATA ANALYSIS

Our target star, π^1 UMa (HD 72905, GJ 311), is a G1.5 V, magnitude $V = 5.64$ star, at a distance of 14.4 pc; with a mass, radius, and temperature of $M = 1.03 M_\odot$, $R = 0.95 R_\odot$, and $T_{\text{eff}} = 5850$ K, respectively (Ribas et al.

* Based on observations made with the NASA/ESA *Hubble Space Telescope*, obtained at the Space Telescope Science Institute, which is operated by the Association of Universities for Research in Astronomy, Inc., under NASA contract NAS 5-26555. These observations are associated with program GO-12596.

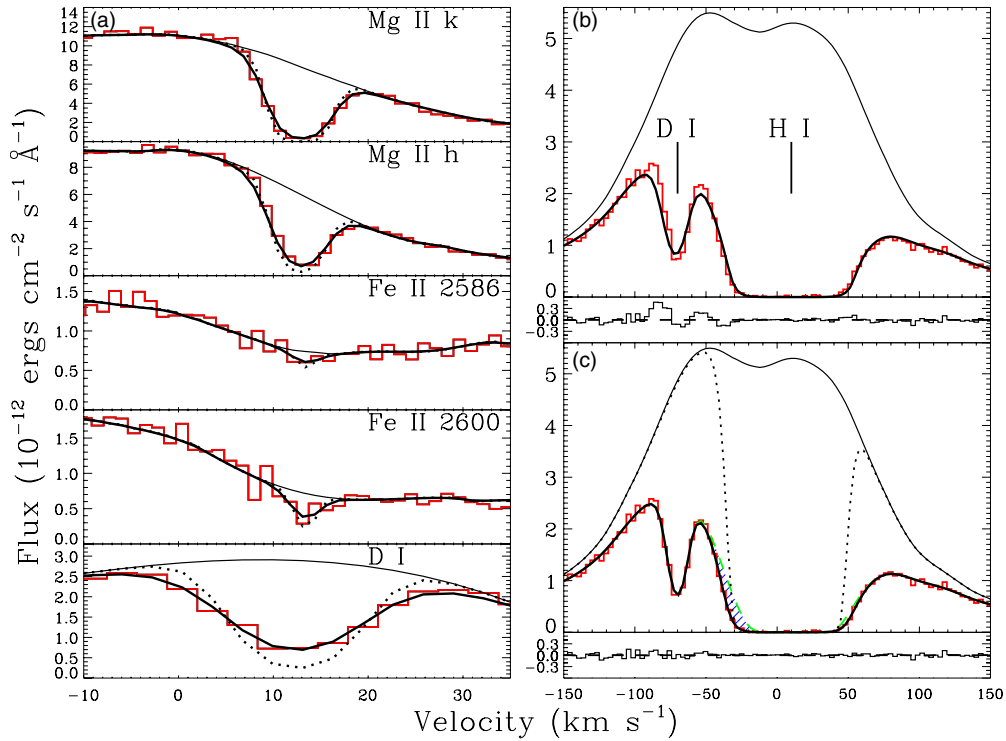


Figure 1. (a) Fits to ISM absorption lines observed by *HST* toward π^1 UMa, plotted on a heliocentric velocity scale, both before (dotted lines) and after (thick solid lines) instrumental smoothing. (b) A fit to the H I + D I Ly α spectrum of π^1 UMa, assuming only ISM absorption is present. The H I and D I absorption are forced to be self-consistent (see text), and the result is a very poor fit, due mostly to H I being blueshifted relative to D I (and the other ISM absorption lines). The upper solid line is the reconstructed stellar Ly α profile. (c) A two-component fit to the Ly α spectrum, representing absorption from the ISM (green dashed line) and from the stellar astrosphere (black dotted line). The combination of the two components (thick black line) fits the data (after instrumental smoothing). The hatched region explicitly indicates the excess absorption due to the astrosphere, beyond the absorption from the ISM.

(A color version of this figure is available in the online journal.)

2005). This is a young, active, rapidly rotating star, with a rotation period of $P_{\text{rot}} = 4.69$ days (Donahue et al. 1996), an average *ROSAT*/PSPC X-ray luminosity of $\log L_X = 28.96$ (Schmitt & Liefke 2004), a chromospheric Ca II activity index of $\langle S \rangle = 0.367$ (Donahue et al. 1996), and an estimated age of 500 ± 100 Myr (King et al. 2003). We observed π^1 UMa with *HST* on 2012 September 25, the observation consisting of a 5626 s exposure of the 1140–1710 Å spectral region using the E140M grating of the Space Telescope Imaging Spectrograph (STIS) instrument. An archival STIS/E230H spectrum from 2010 April 24 is also utilized in our analysis, which includes interstellar absorption lines from Mg II h and k at 2803 Å and 2796 Å, respectively, and Fe II lines at 2586 Å and 2600 Å.

The absorption lines observed toward π^1 UMa are displayed in Figure 1. Figure 1(a) shows the interstellar Mg II, Fe II, and D I (deuterium) Ly α lines. Following procedures from many past analyses (Redfield & Linsky 2002, 2004), the central velocity (v), Doppler broadening parameter (b), and column density (N) suggested by these lines are measured using fits to the lines, including corrections for instrumental broadening (Hernandez et al. 2012). The narrow, symmetric line profiles are indicative of a single velocity component, which is close to the expected $v = 11.9$ km s $^{-1}$ velocity predicted by the Local Interstellar Cloud (LIC) vector of Redfield & Linsky (2008). Fit parameters are listed in Table 1, including χ_v^2 values indicating quality of fit. It is χ_v^2 that is minimized to determine the best fit, and $\chi_v^2 \approx 1$ is expected for a good fit (Bevington & Robinson 1992). Note that the quoted 1σ uncertainties only include random errors induced by the noise in the data and do not include systematic errors

such as uncertainties in the shape of the overlying continuum, which likely dominates the uncertainties in the analysis.

To constrain these fits as much as possible, the lines of a given species are fitted simultaneously, with self-consistent fit parameters. For example, both Mg II h and k lines are fitted simultaneously. There appears to be a small inconsistency in the wavelength calibration of the two Mg II lines, leading to a mediocre fit to the h line in Figure 1(a). We have seen similar inconsistencies in the past with these two lines (e.g., Wood et al. 2014). Note that Table 1 lists the rest wavelengths of both closely separated fine structure components of the D I and H I Ly α lines, but in the figures we show only the combined absorption.

The π^1 UMa Ly α line is displayed in Figure 1(b), showing both very broad H I absorption, and the narrower D I absorption also shown in Figure 1(a). The broad width and extended damping wings of the H I absorption makes analysis of Ly α more complicated than for the absorption lines in Figure 1(a). Our analysis follows procedures developed to study previous Ly α spectra (Wood et al. 2005b). In short, we reconstruct the stellar emission line profile with guidance from the stellar Mg II line profiles in the E230H spectrum, and we initially attempt to fit the data with only ISM absorption. The velocity and Doppler broadening parameters of H I and D I are forced to be self-consistent [meaning $v(\text{H I}) = v(\text{D I})$ and $b(\text{H I}) = \sqrt{2} \times b(\text{D I})$], and we also assume $\text{D}/\text{H} = 1.56 \times 10^{-5}$ (Wood et al. 2004). In effect, this means the fitted H I absorption profile is highly constrained by the much less saturated D I absorption profile. The resulting fit is displayed in Figure 1(b). The fit is quite poor, with $\chi_v^2 = 3.18$, mostly because the H I absorption is blueshifted relative to the D I absorption.

Table 1
Absorption Line Fit Parameters

Ion	λ_{rest}^a (Å)	v^b (km s ⁻¹)	b (km s ⁻¹)	$\log N$ log(cm ⁻²)	χ_v^2
Mg II	2796.3543, 2803.5315	12.83 ± 0.16	2.53 ± 0.08	12.78 ± 0.01	1.12
Fe II	2586.6500, 2600.1729	13.36 ± 0.33	1.43 ± 0.63	12.23 ± 0.10	1.41
D I	1215.3430, 1215.3376	12.49 ± 0.16	6.55 ± 0.27	13.33 ± 0.02	1.84
H I (ISM)	1215.6682, 1215.6736	12.58 ± 0.10	9.35 ± 0.23	18.12 ± 0.01	1.06
H I (astrosphere)	1215.6682, 1215.6736	7.87 ± 0.24	17.64 ± 0.11	15.83 ± 0.03	1.06

Notes.

^a Rest wavelengths of measured lines, in vacuum.

^b Central velocity in a heliocentric rest frame.

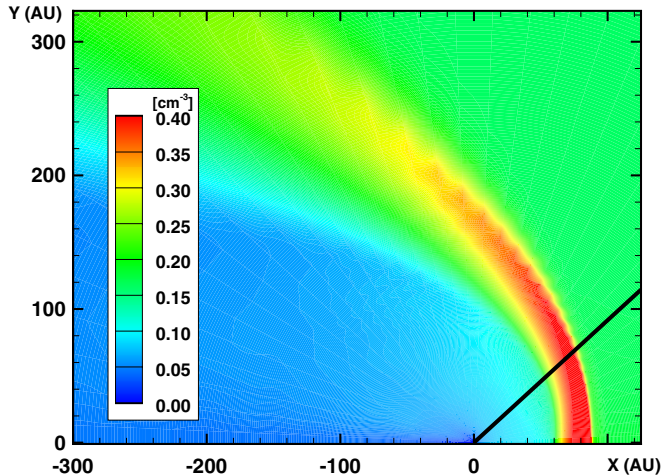


Figure 2. H I density distribution of a hydrodynamic model of the π^1 UMa astrosphere, assuming $\dot{M} = 0.5 \dot{M}_\odot$, which leads to the best fit to the data in Figure 3. The black line indicates our line of sight to the star.

A blueshift of the H I Ly α absorption relative to other ISM absorption lines is an indication of excess H I absorption on the blue side of the line, which is the signature of astrospheric absorption. The blueshifted astrospheric absorption signature is analogous to heliospheric absorption that is sometimes observed on the red side of the line (Wood et al. 2005b). The deceleration and deflection of ISM material as it approaches the heliopause yields a redshifted heliospheric absorption signature; the analogous effect for astrospheres yields blueshifted absorption from our perspective.

In Figure 1(c) we show a fit to the data with two absorption components, an ISM absorption component and a second component meant to (crudely) represent the astrospheric absorption. Parameters of the fit are listed in Table 1. The fit quality is excellent, with $\chi_v^2 = 1.06$. An F test formally shows that this is easily enough of an improvement over the $\chi_v^2 = 3.18$ value of the Figure 1(b) fit to justify the extra free parameters. Note that heliospheric absorption is not expected to be very detectable toward π^1 UMa, since this line of sight is not in an upwind direction relative to the ISM flow seen by the Sun. Nevertheless, the fit in Figure 1(c) actually suggests a slight excess absorption on the red side of the line where the heliospheric absorption would be. The absorption component meant to account for the astrospheric absorption is also contributing some absorption on the red side of the line. We consider this to be too small of an effect to represent a clear detection of heliospheric absorption, but we do note that the excess absorption is roughly

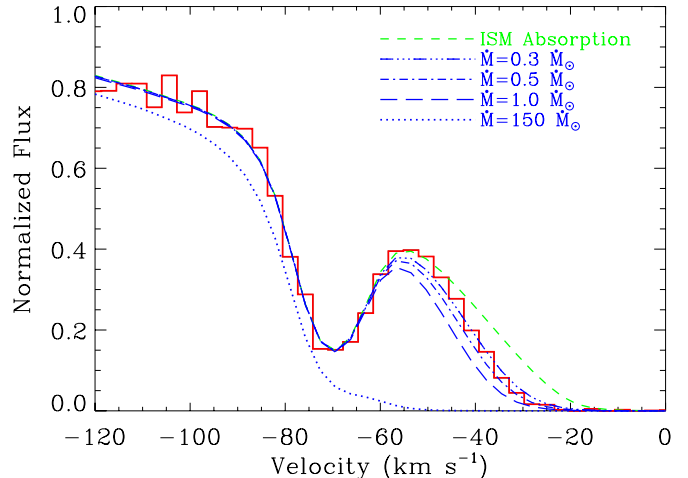


Figure 3. Zooming in on the blue side of the Ly α profile from Figure 1(c), the astrospheric absorption signature is compared with absorption predictions from four hydrodynamic models of the astrosphere, assuming four different mass-loss rates for π^1 UMa (after the astrospheric absorption is added to that of the ISM).

consistent with that expected from the heliosphere based on a heliospheric model that we have previously demonstrated can reproduce more convincing detections of upwind heliospheric absorption (Wood et al. 2000).

As in past analyses (Wood et al. 2002, 2005a), we infer stellar wind strengths from the absorption excess with help from hydrodynamic models of the astrosphere that take into account the ISM wind speed encountered by the star and the orientation of our line of sight through the astrosphere to the star. The known stellar motion vector and known LIC flow vector (Redfield & Linsky 2008) imply that π^1 UMa sees an ISM wind speed of 34 km s⁻¹, and our line of sight to the star is 43° from the upwind direction. Our hydrodynamic models of the π^1 UMa astrosphere are extrapolated from a model that successfully reproduces heliospheric absorption, as described in detail elsewhere (Zank et al. 1996; Wood et al. 2000, 2002), but we change the assumed ISM wind speed to the π^1 UMa value. Mass-loss rates are varied by changing the assumed stellar wind density. Figure 2 shows a model that assumes $\dot{M} = 0.5 \dot{M}_\odot$.

Figure 3 shows absorption predictions from four astrospheric models with four different mass-loss rates. The most important place for the models to fit the data is near the base of the absorption, as discrepancies at higher fluxes away from the base can potentially be mitigated by minor alterations to the assumed stellar Ly α profile. Thus, based on Figure 3 we consider the $0.5 \dot{M}_\odot$ model to be the best fit to the data, though we would consider the $0.3 \dot{M}_\odot$ model to be an acceptable fit as well.

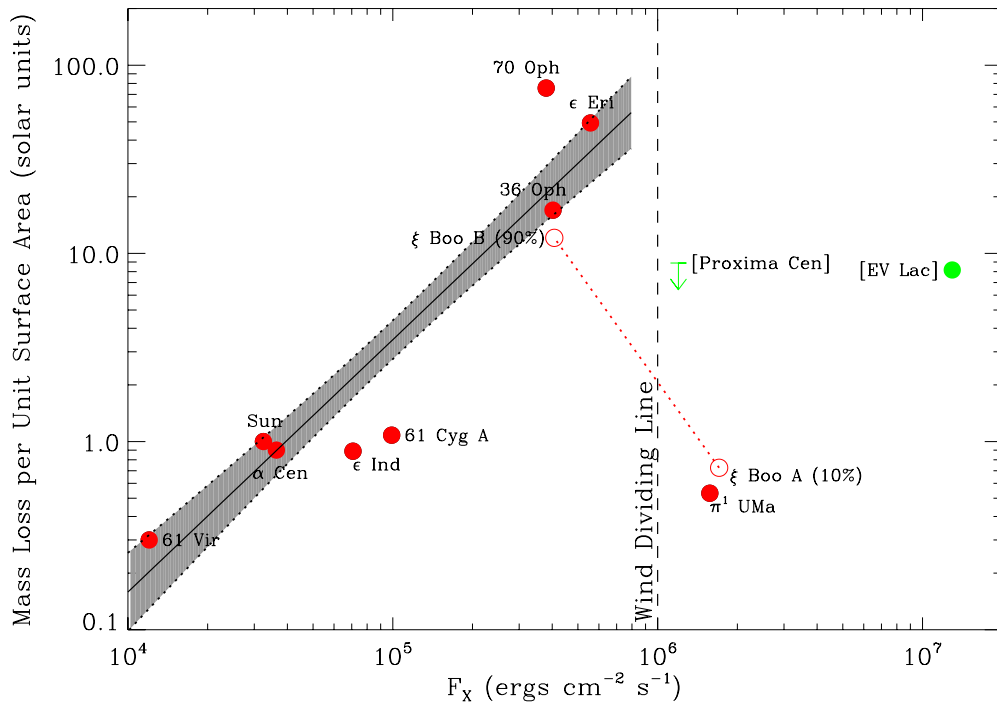


Figure 4. Plot of mass-loss rate (per unit surface area) vs. X-ray surface flux for all main sequence stars with measured winds, analogous to previously published figures (Wood et al. 2002, 2005a), but now with our new π^1 UMa measurement. Red circles are solar-like G and K stars, and green symbols with square-bracketed labels are for two M dwarfs. Separate points are plotted for the two members of the ξ Boo binary, assuming ξ Boo B accounts for 90% of the binary’s wind, and ξ Boo A only accounts for 10%. A power law, $\dot{M} \propto F_X^{1.34 \pm 0.18}$, is fitted to the less active stars where a wind/corona relation seems to exist, but this relation seems to fail for stars to the right of the “Wind Dividing Line” in the figure.

(A color version of this figure is available in the online journal.)

As discussed in past work (Wood et al. 2002, 2005a), we estimate that mass-loss rates measured in this fashion are good to within about a factor of two.

3. DISCUSSION

Our $\dot{M} = 0.5 \dot{M}_\odot$ measurement is dramatically lower than the $\dot{M} = 150 \dot{M}_\odot$ prediction based on the assumption that the solar flare/CME relation can be extrapolated to the far more active π^1 UMa (Drake et al. 2013). Figure 3 shows explicitly just how much astrospheric absorption should have been seen toward π^1 UMa if it had a $\dot{M} = 150 \dot{M}_\odot$ wind. The predicted absorption is so broad that it actually obscures the D I line. Nevertheless, there are scenarios that would allow π^1 UMa to possess a $\dot{M} = 150 \dot{M}_\odot$ wind and still be consistent with the Ly α data, although they require unusual ad hoc assumptions about the nature of the ISM in the vicinity of the star. For example, perhaps π^1 UMa is actually surrounded by a fully ionized ISM and therefore has no detectable astrospheric absorption, with the excess absorption in Figure 3 being not astrospheric in nature but instead a mysterious ISM absorption component with a column density too low to be detectable in Mg II or D I, or, even if the excess absorption is astrospheric, perhaps the ISM characteristics around π^1 UMa are radically different from the assumptions in our models (which assume an ISM like that around the Sun), such that we are grossly underestimating the wind strength. For example, we are able to fit the data reasonably well with $\dot{M} = 150 \dot{M}_\odot$ if we reduce the assumed ISM neutral H density in the model from $n_H = 0.16 \text{ cm}^{-3}$ to $n_H = 0.0024 \text{ cm}^{-3}$ and the proton density from $n_p = 0.08 \text{ cm}^{-3}$ to $n_p = 0.0456 \text{ cm}^{-3}$. However, such unusual ISM conditions with low pressures and/or very low neutral fractions do not seem very likely.

In Figure 4, we plot the mass-loss rate (per unit surface area) versus X-ray surface flux for all main sequence stars with measured winds, analogous to figures published before (Wood et al. 2002, 2005a), but including our new π^1 UMa data point. The G and K stars with $F_X < 10^6 \text{ erg cm}^{-2} \text{ s}^{-1}$ are consistent with winds increasing in strength with activity, and are fitted with a power law relation, $\dot{M} \propto F_X^{1.34 \pm 0.18}$ (Wood et al. 2005a). However, the two GK stars with $F_X > 10^6 \text{ erg cm}^{-2} \text{ s}^{-1}$, including π^1 UMa, have winds much weaker than this relation would predict, leading to the inclusion of a “Wind Dividing Line” in Figure 4, indicating where the wind/X-ray correlation seems to fall apart. For the ξ Boo binary, Figure 4 indicates how the binary’s combined wind strength of $\dot{M} = 5 \dot{M}_\odot$ is most consistent with the other measurements if 90% of the wind is ascribed to ξ Boo B, and only 10% to ξ Boo A.

The mass-loss/activity relation seen for less active stars in Figure 3 appears to fail rather dramatically for $F_X > 10^6 \text{ erg cm}^{-2} \text{ s}^{-1}$, corresponding to a stellar age of about $t = 700 \text{ Myr}$ for solar-like stars (Ayres 1997). Perhaps this is due to a fundamental change in stellar magnetic topology at that time, with the topology of the young, active stars acting to inhibit mass loss (Wood et al. 2005a; Schrijver & Title 2001). This change in character might plausibly be connected to the appearance of large polar starspots commonly found for stars in this very active regime (Strassmeier 2002). It is also possible that the “Wind Dividing Line” is indicative of more fundamental changes in how the magnetic dynamo is operating, analogous to recent interpretations of stellar activity and rotation in young open clusters (Barnes 2003, 2010; Gondoin 2012, 2013). Theoretical modeling of stellar winds may be useful for addressing these issues. A variety of theoretical approaches have recently been applied to the general problem of stellar

wind evolution (Holzwarth & Jardine 2007; Vidotto et al. 2009; Cranmer & Saar 2011; Sterenborg et al. 2011; Suzuki 2013).

The fundamental implication of Figure 4 is that the most active stars do not have particularly strong winds. Not only do the two G dwarfs in the most active regime have unexpectedly weak winds, but there are also two active M dwarfs shown in the figure, Proxima Cen (M5.5 V) and EV Lac (M3.5 V), which also have surprisingly weak winds. In addition, it is worth mentioning that there are two active evolved stars in this high activity regime, λ And (G8 IV-III+M V) and DK UMa (G4 III-IV), that have weak coronal winds of $\dot{M} \leq 5 \dot{M}_{\odot}$ (Wood et al. 2005a). Finally, we note that many of the dozens of astrospheric nondetections are for very active stars (e.g., AU Mic, κ Cet, χ^1 Ori, and many more; Wood et al. 2005b). Individually, a nondetection means little because of the plausible explanation that the star is surrounded by fully ionized ISM, but collectively, the failure to detect any astrospheric absorption for so many active stars qualifies as further evidence that these stars may not have strong winds. In short, if coronal winds of $\dot{M} > 100 \dot{M}_{\odot}$ are common, particularly for active stars, it is becoming increasingly difficult to explain why we are not finding any examples of the expected astrospheric absorption signatures of these massive winds.

Support for program GO-12596 was provided by NASA through an award from the Space Telescope Science Institute, which is operated by the Association of Universities for Research in Astronomy, Inc., under NASA contract NAS 5-26555. E.E. acknowledges support through a NASA undergraduate research fellowship from the Connecticut Space Grant Consortium. This research has made use of the SIMBAD database, operated at CDS, Strasbourg, France.

REFERENCES

- Ayres, T. R. 1997, *JGR*, 102, 1641
 Barnes, S. A. 2003, *ApJ*, 586, 464
 Barnes, S. A. 2010, *ApJ*, 722, 222
 Bevington, P. R., & Robinson, D. K. 1992, *Data Reduction and Error Analysis for the Physical Sciences* (New York: McGraw-Hill)
 Cohen, O. 2011, *MNRAS*, 417, 2592
 Cranmer, S. R. 2012, *SSRv*, 172, 145
 Cranmer, S. R., & Saar, S. H. 2011, *ApJ*, 741, 54
 Denissenkov, P. A. 2010, *ApJ*, 719, 28
 Donahue, R. A., Saar, S. H., & Baliunas, S. L. 1996, *ApJ*, 466, 384
 Drake, J. J., Cohen, O., Yashiro, S., & Gopalswamy, N. 2013, *ApJ*, 764, 170
 Gallet, F., & Bouvier, J. 2013, *A&A*, 556, A36
 Gayley, K. G., Zank, G. P., Pauls, H. L., Frisch, P. C., & Welty, D. E. 1997, *ApJ*, 487, 259
 Gondoin, P. 2012, *A&A*, 546, A117
 Gondoin, P. 2013, *A&A*, 556, A14
 Hernandez, S., Aloisi, A., Bohlin, R., et al. 2012, *STIS Instrument Handbook Ver. 12.0* (Baltimore, MD: STSci)
 Holzwarth, V., & Jardine, M. 2007, *A&A*, 463, 11
 Irwin, J., Hodgkin, S., Aigrain, S., et al. 2007, *MNRAS*, 377, 741
 Khodachenko, M. L., Alexeev, I., Belenkaya, E., et al. 2012, *ApJ*, 744, 70
 King, J. R., Villarreal, A. R., Soderblom, D. R., Gulliver, A. F., & Adelman, S. J. 2003, *AJ*, 125, 1980
 Lallement, R., Welsh, B. Y., Vergely, J. L., Crifo, F., & Sfeir, D. 2003, *A&A*, 411, 447
 Lammer, H. L., Selsis, F., Chassefière, E., et al. 2010, *AsBio*, 10, 45
 Linsky, J. L., & Wood, B. E. 1996, *ApJ*, 463, 254
 Parker, E. N. 1958, *ApJ*, 128, 664
 Redfield, S., & Linsky, J. L. 2002, *ApJS*, 139, 439
 Redfield, S., & Linsky, J. L. 2004, *ApJ*, 602, 776
 Redfield, S., & Linsky, J. L. 2008, *ApJ*, 673, 283
 Ribas, I., Guinan, E. F., Güdel, M., & Audard, M. 2005, *ApJ*, 622, 680
 Schmitt, J. H. M. M., & Liefke, C. 2004, *A&A*, 417, 651
 Schrijver, C. J., & Title, A. M. 2001, *ApJ*, 551, 1099
 Spada, F., Lanzafame, A. C., Lanza, A. F., Messina, S., & Collier Cameron, A. 2011, *MNRAS*, 416, 447
 Sterenborg, M. G., Cohen, O., Drake, J. J., & Gombosi, T. I. 2011, *JGR*, 116, A01217
 Strassmeier, K. G. 2002, *AN*, 323, 309
 Suzuki, T. K. 2013, *AN*, 334, 81
 Terada, N., Kulikov, Y. N., Lammer, H., et al. 2009, *AsBio*, 9, 55
 Vidotto, A. A., Opher, M., Jatenco-Pereira, V., & Gombosi, T. I. 2009, *ApJ*, 699, 441
 Wood, B. E., Izmodenov, V. V., Alexashov, D. B., Redfield, S., & Edelman, E. 2014, *ApJ*, 780, 108
 Wood, B. E., & Linsky, J. L. 2010, *ApJ*, 717, 1279
 Wood, B. E., Linsky, J. L., Hébrard, G., et al. 2004, *ApJ*, 609, 838
 Wood, B. E., Müller, H. -R., & Zank, G. P. 2000, *ApJ*, 542, 493
 Wood, B. E., Müller, H. -R., Zank, G. P., & Linsky, J. L. 2002, *ApJ*, 574, 412
 Wood, B. E., Müller, H. -R., Zank, G. P., Linsky, J. L., & Redfield, S. 2005a, *ApJL*, 628, L143
 Wood, B. E., Redfield, S., Linsky, J. L., Müller, H. -R., & Zank, G. P. 2005b, *ApJS*, 159, 118
 Zank, G. P., Pauls, H. L., Williams, L. L., & Hall, D. T. 1996, *JGR*, 101, 21639